ACS APPLIED MATERIALS & INTERFACES

Research Article

www.acsami.org

Structural and Optical Characterization of ZnO/$Mg_xZn_{1-x}O$ Multiple Quantum Wells Based Random Laser Diodes

Qike Jiang,[†] He Zheng,[†] Jianbo Wang,*[,†] Hao Long,[‡] and Guojia Fang*[,‡]

[†]School of Physics and Technology, Center for Electron Microscopy and MOE Key Laboratory of Artificial Micro- and Nano-structures, Wuhan University, Wuhan 430072, People's Republic of China

[‡]Department of Electronic Science & Technology, School of Physics and Technology and MOE Key Laboratory of Artificial Micro- and Nano-structures, Wuhan University, Wuhan 430072, People's Republic of China

Supporting Information

ABSTRACT: Two kinds of laser diodes (LDs) comprised of ZnO/$Mg_xZn_{1-x}O$ (ZnO/MZO) multiple quantum wells (MQWs) grown on GaN (MQWs/GaN) and Si (MQWs/Si) substrates, respectively, have been constructed. The LD with MQWs/GaN exhibits ultraviolet random lasing under electrical excitation, while that with MQWs/Si does not. In the MQWs/Si, ZnO/MZO MQWs consist of nanoscaled crystallites, and the MZO layers undergo a phase separation of cubic MgO and hexagonal ZnO. Moreover, the Mg atom predominantly locates in the MZO layers along with a significant aggregation at the ZnO/MZO interfaces; in sharp contrast, the ZnO/MZO MQWs in the MQWs/GaN show a well-crystallized structure with epitaxial relationships among GaN, MZO, and ZnO. Notably, Mg is observed to diffuse into the ZnO well layers. The structure−optical property relationship of these two LDs is further discussed.

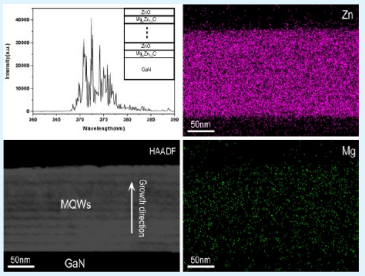

KEYWORDS: *random laser diode, multiple quantum wells, ZnO/$Mg_xZn_{1-x}O$, TEM*

1. INTRODUCTION

As a semiconductor material with direct and wide band gap (E_g = 3.37 eV) at room temperature (RT),[1] ZnO can be potentially employed for ultraviolet (UV) lasing. Its large exciton binding energy (60 meV), which is much larger than the thermal energy (~26 meV) at RT, could lead to lasing action based on exciton recombination even above RT. Besides, ZnO exhibits excellent chemical and thermal stability, specific electrical and optoelectronic properties. Thus, it is considered as a promising material for the next generation of short-wavelength light-emitting diodes (LEDs) and laser diodes (LDs) which have been extensively employed in various domains, including lighting, display, high-density data storage, and medical fields.[2]

Theoretically, by alloying ZnO with various concentrations of MgO, the energy band gap of ternary alloy $Mg_xZn_{1-x}O$ (MZO) could be tuned from 3.37 to 7.7 eV,[3] making the MZO alloy the potential wide band gap material for possible applications in optoelectronic devices. However, according to the phase diagram of the ZnO−MgO binary system, the thermodynamic solubility limit of MgO in the ZnO matrix has been reported to be less than 4 at. %.[4] Hence, to modulate the energy band gap, one needs to increase the Mg content in the MZO thin film which is associated with the risk that the MZO alloy could undergo the phase separation of cubic MgO and hexagonal ZnO with high Mg content or high temperature (above 700 °C).[5] Various growth methods, such as pulsed laser deposition (PLD), molecular beam epitaxy (MBE), and metal−organic chemical vapor deposition (MOCVD), etc., have been employed to grow stable MZO thin films with controllable higher x (i.e., higher Mg content)[6−9] and thus to effectively increase the energy band gap. These achievements make it possible to fabricate LEDs and LDs based on ZnO/MZO multiple quantum wells (MQWs) which can facilitate radiative recombination by carrier confinement.[10−12]

In this paper, we have constructed two kinds of random LDs based on ZnO/MZO MQW structure. Their optical properties are studied by electroluminescence (EL) spectra. Their microstructures, including the morphology, crystalline states, crystallographic relationship, and compositional distribution, are systematically investigated by means of transmission electron microscopy (TEM). The probable correlation between the structure and optical behaviors in the LDs is discussed.

2. EXPERIMENTAL SECTION

Two sets of ten periods of ZnO/MZO MQWs were first grown on Si and GaN wafers at 300 °C with optimized growth condition by the radio frequency (rf) magnetron sputtering system. The electron concentrations of Si and GaN are ~10^{18} cm^{-3}. The MQW structures are schematically illustrated in the insets of Figure 1a,b. Then, the MQW structures were assembled with p-type NiO and Au and In electrodes to form the final LDs. The hole concentration of NiO is ~10^{19} cm^{-3}. The fabrication details can be found elsewhere.[10] The RT electroluminescence measurement was carried out by an Acton SpectraPro 2500i monochromator. Cross-sectional specimens suitable for transmission electron microscopy examination were prepared by mechanical polishing and subsequent Ar ion beam thinning. In particular, the as-deposited samples were first cut into slices with size

Received: October 18, 2012
Accepted: November 27, 2012
Published: November 27, 2012

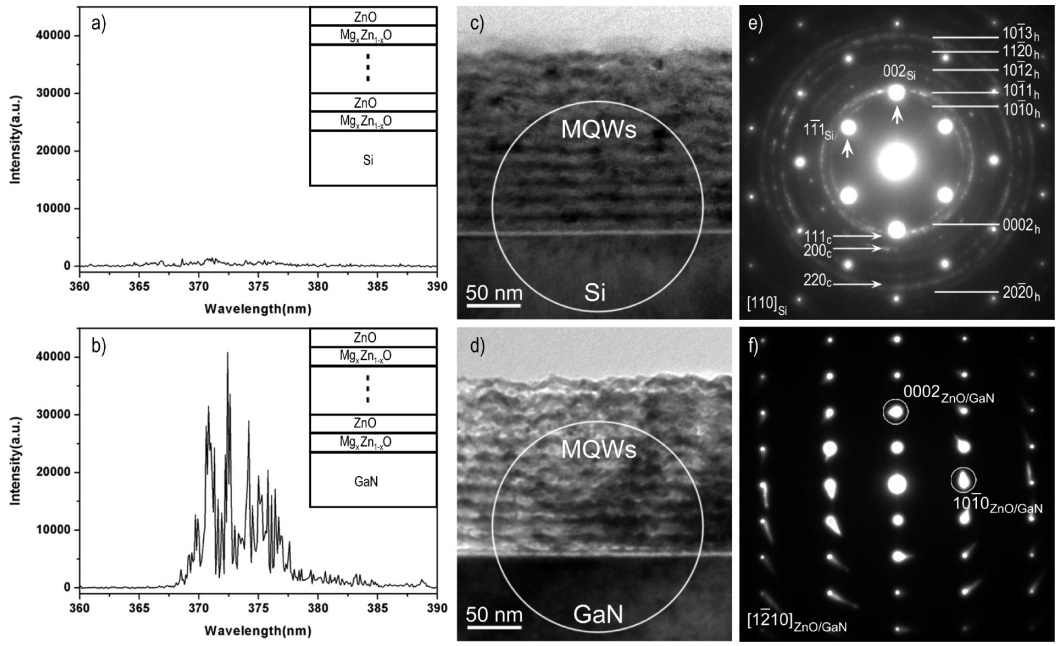

Figure 1. (a) and (b) RT EL spectra in the wavelength range from 360 to 390 nm of the MQWs/Si and MQWs/GaN based LDs, respectively. The forward bias is 5.0 V. Insets are the corresponding schematic illustrations of ZnO/MZO MQW structures grown on Si and GaN substrates. (c) and (d) BF images of MQWs/Si and MQWs/GaN structures. (e) SAED pattern obtained from the circled area of (c). Subscripts "h" and "c" denote hexagonal ZnO and cubic MgO phases, respectively. (f) SAED pattern obtained from the circled area of (d).

of 2.5 × 2.5 mm. Subsequently, four of these slices were adhered to form a sandwiched structure, which underwent mechanical polishing. Then, samples were thinned in a Gatan Model 691 Precise Ion Polishing System operated at 4.5 keV. Conventional selected area electron diffraction (SAED) patterns and bright field (BF) images were obtained by using a JEOL JEM-2010 (HT) electron microscope. High-resolution transmission electron microscopy (HRTEM) images, high-angle annular dark field (HAADF) Z-contrast images, energy dispersive X-ray spectroscopy (EDS) spectrum, and elemental maps were conducted by using a JEOL JEM-2010FEF (UHR) electron microscope. All microscopes were operated with an acceleration voltage of 200 kV.

3. RESULTS AND DISCUSSION

First, the RT EL spectra in the wavelength ranging from 360 to 390 nm were achieved with a forward bias of 5.0 V, which indicates distinct optical behaviors of the two kinds of LDs: some discrete sharp lasing peaks in the UV region are observed in the spectrum of MQWs/GaN based LD as shown in Figure 1b (more information can be found in ref 10), while no obvious lasing action could be found in the spectrum of MQWs/Si based LD as presented in Figure 1a (a detailed spectrum with reduced range of vertical axis can be seen in Figure S1 of the Supporting Information). Considering the only variation of these two LDs is the choice of substrate, we perform the detailed structural analysis to reveal the probable underlying mechanism.

Figure 1c,d is cross-sectional images of the MQWs/Si and MQWs/GaN structures, respectively. The thicknesses of the ZnO/MZO MQWs are both about 170 nm. The interfaces between the ZnO and MZO layers are clearly visible. Evidently, both images show ten periods of ZnO and MZO layers with dark and bright contrasts, respectively. It is worth noting that the structure of several outermost layers was damaged as a result of the Ar ion milling. Figure 1e shows the SAED pattern obtained from the circled area of Figure 1c. The major diffraction spots could be indexed according to the Si structure, i.e., [110] zone axis. Obviously, the MQWs were sputtered on the Si(001) plane. Besides the Si diffraction spots, there exist the diffraction rings, implying the polycrystalline structure of ZnO/MZO MQWs. The polycrystalline MQW structure should be the result of large lattice mismatch (40%) between ZnO and Si[13] and relatively lower growth temperature (300 °C). Moreover, these rings cannot be indexed as pure hexagonal ZnO phase, and the extra discontinuous diffraction rings can be indexed as cubic MgO phase (JCPDS 87-0653) (Figure 1e). The appearance of the cubic MgO phase suggests that a phase separation occurred when MQWs were sputtered on the Si substrate, especially inside the MZO layers. In contrast, no diffraction rings were presented in the SAED pattern (Figure 1f) obtained from the MQWs/GaN structure (circled area of Figure 1d), indicating that the ZnO can coherently epitaxy on the GaN substrate due to the small in-plane lattice mismatch between ZnO and GaN (1.8%). As a result, the SAED pattern only consists of diffraction spots corresponding to hexagonal ZnO and GaN phases (Figure 1f). The crystallographic relationships deducted from Figure 1f are $[1\bar{2}10]_{GaN}//[1\bar{2}10]_{MZO}//[1\bar{2}10]_{ZnO}$, $(0001)_{GaN}//(0001)_{MZO}//(0001)_{ZnO}$, and $(10\bar{1}0)_{GaN}//(10\bar{1}0)_{MZO}//(10\bar{1}0)_{ZnO}$.

Furthermore, HRTEM analysis has been carried out to reveal the detailed structural information. Figure 2a shows the HRTEM image of the MQWs/Si structure with the electron beam parallel to the [110] zone axis of Si. A native amorphous SiO_2 layer with a thickness of about 5 nm is observed between Si and ZnO layers. This continuous amorphous layer commonly occurred during the rf magnetron sputtering process under ambient oxygen.[14,15] Periods of MZO and ZnO layers sequentially appear in the form of nanoscaled crystallites, and the fluctuant interfaces between different layers can be easily distinguished from the contrast difference. The inset is the corresponding fast Fourier transform (FFT) pattern obtained from the MQW area, whereas the ring-like pattern verifies again the polycrystalline nature of MQWs. In comparison, Figure 2b

dx.doi.org/10.1021/am302378v | ACS Appl. Mater. Interfaces 2012, 4, 7043−7046

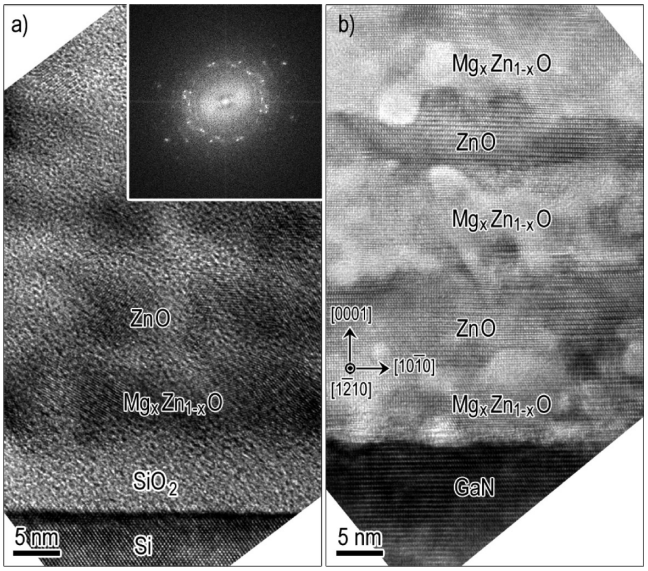

Figure 2. (a) and (b) HRTEM images of MQWs/Si and MQWs/GaN structures, respectively.

displays the HRTEM image of the MQWs/GaN structures along the [1$\bar{2}$10] direction of ZnO and GaN, representing the coherent GaN/MZO and MZO/ZnO interfaces, which further confirms the epitaxy relationships among GaN, MZO, and ZnO.

Aiming to reveal the detailed element distribution in the ZnO/MZO MQWs structure, HAADF imaging has been performed. Figures 3a and 4a present the HAADF images of MQWs/Si and MQWs/GaN structures, correspondingly. The composition difference between ZnO and MZO layers is reflected by the different contrasts between these two kinds of layers. In principle, the HAADF image can be referred to as *Z*-contrast (where *Z* is an atomic number) image because each column of the image follows approximately the expected Z^2 dependence of the Rutherford scattering cross section.[16] Since heavier elements scatter more, ZnO well layers exhibit brighter contrast than that of MZO layers as shown in Figures 3a and 4a. The smooth interfaces between ZnO and MZO layers in MQWs/GaN (Figure 4a) as compared with that of MQWs/Si imply the different crystalline states of the ZnO/MZO layers as discussed above (Figure 1c–f).

Simultaneously, the EDS spectra of these MQWs/Si and MQWs/GaN structures are shown in Figures 3b and 4b, respectively, based upon which the Zn, Mg, and O are presented in both MQWs. In subsequence, elemental maps of MQWs/Si and MQWs/GaN were constructed by employing the Zn and Mg signals, respectively. In the MQWs/Si structure (Figure 3c,d), the ZnO well layers and MZO barrier layers are quite distinct from each other. By applying intensity profiles across the MQWs/Si structure, the distribution of Zn and Mg elements could be well understood. Figure 3e,f indicates the intensity profiles acquired by scanning the enclosed areas along the growth direction in Figure 3c,d, correspondingly. The curves reflect the local elemental distribution, while purple (Figure 3e) and green bands (Figure 3f) are applied to illustrate ZnO and MZO layers, respectively. It is clearly seen that the positions with higher Zn intensity correspond to lower Mg intensity and vice versa. Mg is mainly restricted in the MZO barrier layers as shown in Figure 3f. Interestingly, significant Mg intensity increases at the ZnO/MZO interfaces as indicated by

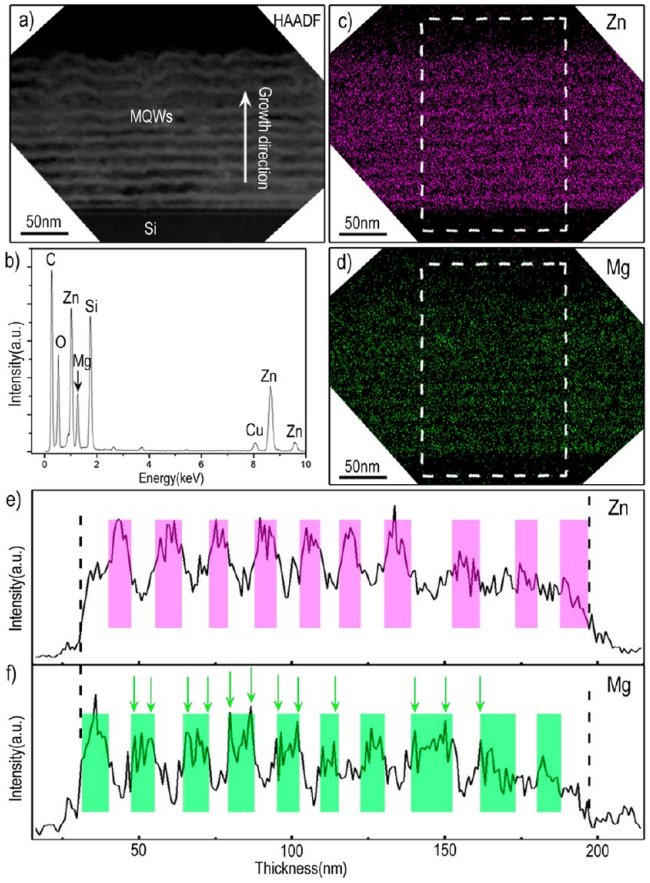

Figure 3. (a) HAADF image of MQWs/Si structure. (b) Corresponding EDS spectrum. (c) and (d) Composite elemental maps of Zn and Mg, respectively. (e) and (f) Intensity profiles obtained by scanning the boxed areas along the growth direction in (c) and (d), respectively.

green arrowed peaks, which implies that Mg aggregation mostly occurred at these interfaces; in other words, the phase separation according to the SAED pattern analysis (Figure 1e) would predominantly take place at the ZnO/MZO interfaces. In the case of MQWs/GaN, composite elemental maps (Figure 4c,d) were also constructed from the Zn and Mg signals. Corresponding intensity profiles (Figure 4e,f) were obtained by scanning the boxed area shown in Figure 4c,d with the same routine mentioned previously. As indicated by green arrows in Figure 4f, a notable Mg element which was supposed to be confined in the MZO barrier layers diffused into ZnO well layers during the fabrication process. According to the growth conditions, the content of Mg could be estimated to be $x \sim 0.15$,[17] which is larger than the solubility limit of MgO in ZnO ($x = 0.04$).[4] Regarding the MQWs/Si structure, it is believed that Mg is not capable of crossing the boundaries between ZnO and MZO layers, neither of the grain boundaries in the MZO layers as a result of the polycrystalline nature. Thus, Mg segregated, and phase separation occurred. In contrast, in the MQWs/GaN structure, Mg can easily pass through the interfaces of ZnO and MZO due to the coherent orientation under sufficient temperature (300 °C), and it can substitute the Zn sites of the ZnO matrix in the MZO layers on the benefit of similar ionic radius between Mg^{2+} (0.57 Å) and Zn^{2+} (0.60 Å).[18]

Such structural characteristics may play a pivotal role in the optical properties of ZnO/MZO MQW based LDs: First, in the

dx.doi.org/10.1021/am302378v | ACS Appl. Mater. Interfaces 2012, 4, 7043–7046

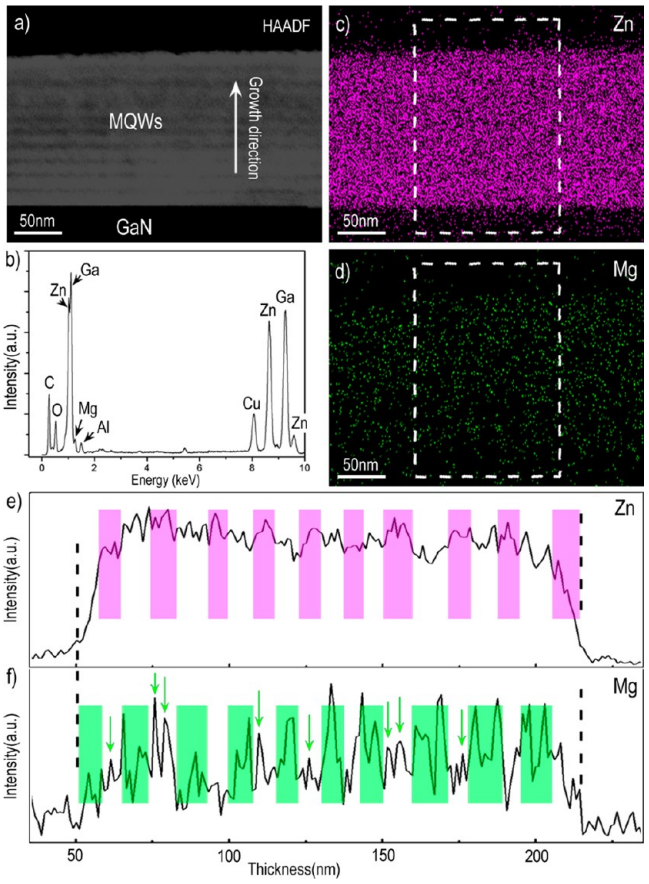

Figure 4. (a) HAADF image of MQWs/GaN structure. (b) Corresponding EDS spectrum. (c) and (d) Composite elemental maps of Zn and Mg, respectively. (e) and (f) Intensity profiles obtained by scanning the boxed areas along the growth direction in (c) and (d), respectively.

MQWs/Si structure, phase separation substantially brings down the band gap of the MZO barrier layer,[8] which makes it impossible to confine carriers and form excitons. As a result, there is no lasing action of the MQWs/Si based diode device. On the other hand, the MZO barrier layers in MQWs/GaN can effectively restrict the motion of carriers due to its well-crystallized structure. The injected electrons and holes quickly form excitons and become localized around the ZnO quantum wells when the diode is forward biased. At enough forward bias, carriers injected into the junction result in exciton−exciton inelastic collisions, which dissociate the localized excitons to form carrier population inversion conditions for stimulated emissions. Second, multiple light scatterings may form close loops to establish gain.[19] In some cases, the emitted light may return to a scattering path, from which it was scattered before, resulting in the formation of a closed-loop resonant cavity. Once the optical gain of the emitted light exceeds the loss in the closed-loop under enough bias voltage, random lasing action could occur.

4. CONCLUSION

In summary, UV random lasing is observed from a MQWs/GaN based LD. The effectively alloyed MZO is believed to act as barrier layers to confine carriers which are essential for the realization of lasing. Conversely, the failure of lasing in MQWs/Si based LDs is mainly ascribed to the polycrystalline nature of ZnO/MZO MQWs, especially in the MZO barrier layers, where phase separation happened. In this case, the electron and hole can pass through the whole MQWs and cannot form excitons, so no lasing action could be observed. Our results shed light on the long-going issue regarding the structure−optical property relationship in LDs and have implications for the better design of optoelectronic devices.

■ ASSOCIATED CONTENT

Supporting Information

Figure S1. This material is available free of charge via the Internet at http://pubs.acs.org.

■ AUTHOR INFORMATION

Corresponding Author

*E-mail: wang@whu.edu.cn (J.W.); gjfang@whu.edu.cn (G.F.).

Notes

The authors declare no competing financial interest.

■ ACKNOWLEDGMENTS

This work was supported by 973 Program (2011CB933300), National Natural Science Foundation of China (51071110, 40972044, 51271134, J1210061), China MOE NCET Program (NCET-07-0640), MOE Doctoral Fund (20090141110059), and the Fundamental Research Funds for the Central Universities.

■ REFERENCES

(1) Özgür, U.; Alivov, Y. I.; Liu, C.; Teke, A.; Reshchikov, M. A.; Doğan, S.; Avrutin, V.; Cho, S. J.; Morkoç, H. J. *Appl. Phys.* **2005**, *98*, 041301..
(2) Service, R. F. *Science* **1997**, *276*, 895.
(3) Chen, N. B.; Sui, C. H. *Mater. Sci. Eng., B* **2006**, *126*, 16−21.
(4) Sarver, J. F.; Katnack, F. L.; Hummel, F. A. J. *Electrochem. Soc.* **1959**, *106*, 960−963.
(5) Ohtomo, A.; Shiroki, R.; Ohkubo, I.; Koinuma, H.; Kawasaki, M. *Appl. Phys. Lett.* **1999**, *75*, 4088−4090.
(6) Park, W. I.; Yi, G. C.; Jang, H. M. *Appl. Phys. Lett.* **2001**, *79*, 2022−2024.
(7) Ohtomo, A.; Kawasaki, M.; Koida, T.; Masubuchi, K.; Koinuma, H.; Sakurai, Y.; Yoshida, Y.; Yasuda, T.; Segawa, Y. *Appl. Phys. Lett.* **1998**, *72*, 2466−2468.
(8) Bhattacharya, P.; Rasmi, R. D.; Katiyar, R. S. *Appl. Phys. Lett.* **2003**, *83*, 2010−2012.
(9) Zhu, J.; Kuznetsov, A. Y.; Han, M. S.; Park, Y. S.; Ahn, H. K.; Ju, J. W.; Lee, I. H. *Appl. Phys. Lett.* **2007**, *90*, 211909.
(10) Long, H.; Fang, G.; Li, S.; Mo, X.; Wang, H.; Huang, H.; Jiang, Q.; Wang, J.; Zhao, X. *IEEE Electron Device Lett.* **2011**, *32*, 54−56.
(11) Park, W. I.; Yi, G. C.; Kim, M.; Pennycook, S. J. *Adv. Mater.* **2003**, *15*, 526−529.
(12) Sun, H. D.; Makino, T.; Segawa, Y.; Kawasaki, M.; Ohtomo, A.; Tamura, K.; Koinuma, H. *Appl. Phys. Lett.* **2001**, *78*, 3385−3387.
(13) Sun, H.; Zhang, Q.; Wu, J. *Nanotechnology* **2006**, *17*, 2271−2274.
(14) Choy, J. H.; Jang, E. S.; Won, J. H.; Chung, J. H.; Jang, D. J.; Kim, Y. W. *Adv. Mater.* **2003**, *15*, 1911−1914.
(15) Jiang, X.; Jia, C. L.; Szyszka, B. *Appl. Phys. Lett.* **2002**, *80*, 3090−3092.
(16) Pennycook, S. J.; Jesson, D. E. *Ultramicroscopy* **1991**, *37*, 14−38.
(17) Fang, G. J.; Li, D. J.; Zhao, X. Z. *Phys. Status Solidi A* **2003**, *200*, 361−368.
(18) Shannon, R. *Acta Crystallogr. A* **1976**, *32*, 751−767.
(19) Ma, X.; Pan, J.; Chen, P.; Li, D.; Zhang, H.; Yang, Y.; Yang, D. *Opt. Express* **2009**, *17*, 14426−14433.